RSC Advances

RSC Advances

www.rsc.org/advances

ROYAL SOCIETY OF CHEMISTRY

www.rsc.org/advances

Graphical Abstract

Simple green synthesis of metal nanoparticles and their composites for antibacterial applications

Simple green method for preparation of Ag NPs and GO+IO+Ag nanocomposites using cinnamon extract developed. The nanocomposites developed are magnetic and as effective as Ag NPs against bacteria and are cheaper due to less amount of Ag.

RSC Advances
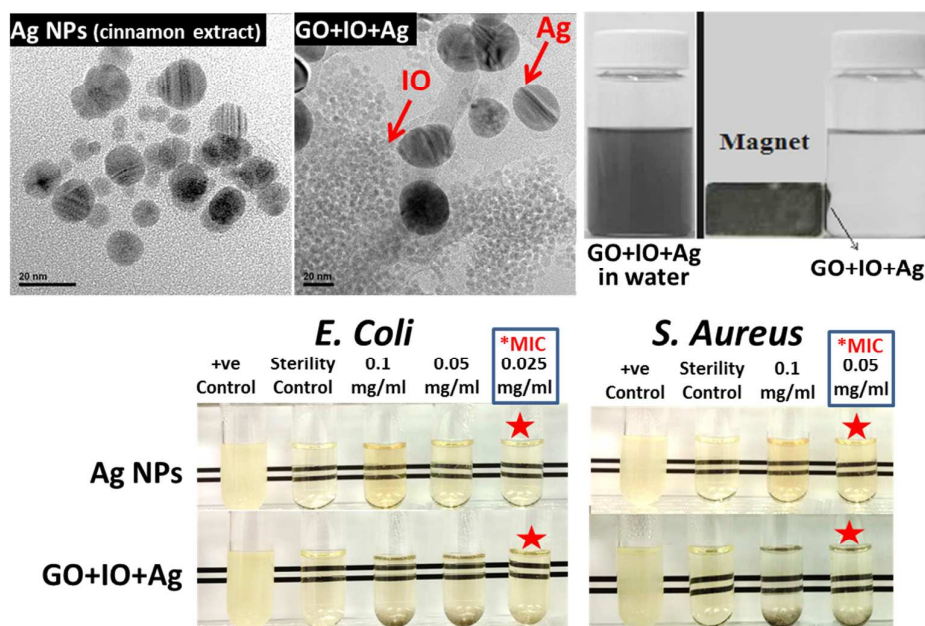
ARTICLE

Synthesis of antibacterial and magnetic nanocomposites by decorating graphene oxide surface with metal nanoparticles

Razieh Moosavi[a,b], Sahana Ramanathan[a,c,d], Yeong Yuh Lee[a], Karen Chong Siew Ling[a], Abbas Afkhami[b], Govindaraju Archunan[d], Parasuraman Padmanabhan[c], Balázs Gulyás[c], Mitali Kakran*[a] and Subramanian Tamil Selvan*[a]

Silver is known to have inhibitory and bactericidal effects. In the present work, we have devised a facile method for the synthesis of metallic silver nanoparticles (Ag NPs) using water-soluble plant extract of cinnamon as a green reducing and capping agent. The formation of Ag NPs was confirmed by the surface plasmon resonance (SPR) absorption at 430 nm in the UV–vis spectra. Different nanocomposites of graphene oxide (GO) with both Ag and iron oxide (IO) NPs exhibiting both antimicrobial and magentic properties were prepared and characterized by UV–vis absorption, Fourier transform infrared (FTIR) and energy-dispersive X-ray (EDX) spectroscopies, and transmission electron microscopy (TEM). The sizes of Ag and IO NPs on GO sheet as determined from the TEM images were 20 and 5 nm, respectively. The antibacterial effects of Ag NPs and [GO+IO+Ag] nanocomposites towards both Gram-negative bacteria *E. coli* and Gram-positive bacteria *S. aureus* were compared. The Ag NPs are mainly responsible for the anitbacterial effects, although GO and IO NPs also possess antibacterial properties. The minimum inhibitory concentration (MIC) values for both Ag NPs and nanocomposites against *E. coli* and *S. aureus* were 0.025 mg/ml and 0.05 mg/ml, respectively. We have also demonstrated that [GO+IO+Ag] nanocomposites are bifunctional (antibacterial and magnetic) and can be harvested with a magnet.

1. Introduction

The ability of pathogenic bacteria to resist current antibiotics has become a serious problem in public health. Therefore, new antibiotics, especially nanomaterials, have been increasingly developed.[1,2] Most of the conventional antibiotics penetrate into and target specific signalling pathways in bacteria, such as breakage of double-stranded DNA, blockage of cell division and triggering of the intrinsic autolysins. Since, they do not physically damage the cell wall, the bacterial morphology is preserved. Because of this the

bacteria can develop resistance.[3] In contrast, metal nanoparticles (NPs) do not have a specific target in bacteria, and they interact with bacterial membranes based on electrostatic interaction, thereby inducing damage by forming pores in the membranes. This physical action prevents bacteria from developing resistance, and promotes lysis of multidrug-resistant bacteria.

In recent years, silver-based antimicrobials have garnered a lot of attention owing to their great antibacterial activity, broad antimicrobial spectrum and low propensity to induce bacteria resistance.[4-6] Silver nanoparticles (Ag NPs) have been shown to be effective against the multi-drug resistant bacteria.[7-9] One of the key characteristic of Ag NPs is that at low concentration they are toxic to microbes but safe for human cells.[10-12] Ag NPs interact with the bacterial cell wall and disrupt the membrane integrity and destroy the DNA replication ability.[13,14] They can directly integrate into the cell membrane and successively form pores, causing an osmotic collapse and release of intracellular materials.[15,16] However, there are challenges associated with the oxidization and aggregation of Ag NPs which limit their practical applications. These are important parameters affecting the antibacterial activity of Ag NPs. These difficulties can be overcome by using graphene oxide (GO) as a substrate to grow Ag NPs to enhance their stability and

a. *Institute of Materials Research and Engineering, A*STAR, 3 Research Link, Singapore, 117602. Tel: +65 68745249; E-mail: subramaniant@imre.a-star.edu.sg (S. T. Selvan), kakranm@imre.a-star.edu.sg (M. Kakran)*
b. *Faculty of Chemistry, Bu-Ali Sina University, 65174 Hamedan, Iran*
c. *Lee Kong Chian School of Medicine, Nanyang Technological University, Singapore 308232*
d. *Centre for Pheromone Technology, Department of Animal Science, Bharathidasan University, Tiruchirappalli – 620 024, Tamil Nadu, India*

antibacterial activity. Gao *et al.* have reported that the presence of GO not only slows down Ag NP oxidation process but also enables Ag^+ ions recrystallization on the GO surface.[17] Besides, GO also acts as a substrate to grow other NPs of interest, such as iron oxide, to form multifunctional nanocomposites.

Individual graphene or GO and graphene-based composites have recently been used against bacteria.[18-22] Hu *et al.* reported that the water-dispersible graphene derivatives, GO and reduced graphene oxide (rGO) nanosheets, can effectively inhibit the growth of *E. coli* bacteria while showing minimal cytotoxicity.[18] Liu *et al.* compared the antibacterial activity of four types of graphene-based materials [graphite (Gt), graphite oxide (GtO), GO, and rGO] towards *E. coli*.[23] According to them, under similar concentration and incubation conditions, GO dispersion showed the highest antibacterial activity, sequentially followed by rGO, Gt, and GtO. Lately, synthesis and application of iron oxide (IO) NPs has been developed extensively[24-26] due to their unique and recyclable properties.[27-30] IO NPs have also shown moderate antimicrobial activity. Magnetic characteristic has considerable capability to kill bacteria that can be readily trapped in a small volume using an external magnet. These properties designate the IO NPs to be used in applications such as clinical infections, and local and direct antimicrobial therapy without posing a risk for human body and its subsequent removal by means of an external magnetic field.[31-36] Using an external magnetic field, IO NPs can be controlled and directed as required throughout the body to kill bacteria.[34-35]

Nanoparticles (NPs) can be produced by many physical and chemical methods, including physical adsorption, surface deposition, arc discharge, plasma polymerization, laser CVD and emulsion polymerization. But these methods use toxic chemicals as reducing agent and stabilizing agent, organic solvents or non-biodegradable agents. For metal NPs to be used for biomedical applications there is an increasing need to develop eco-friendly process without any toxic chemicals. Therefore, the first objective of our study is to develop a simple and green method for the synthesis of Ag NPs. To achieve this, we have employed cinnamon extract as a green reducing agent. Cinnamon powder is commercially economic and abundantly available. In addition, antimicrobial characteristics of cinnamon extracts have been reported and it has been shown to inhibit the growth of both Gram-positive and Gram-negative food borne pathogens or spoilage bacteria, yeast, and molds.[37] Cinnamon is widely used as a condiment and flavouring agent in cooking. Due to its abundant applications, the commercial production of cinnamon powder is quite high, exhibiting a broader availability for the synthesis of Ag NPs.

Another objective of our study is to prepare the nanocomposites of GO with both Ag and IO NPs with the aim to impart magnetic and antibacterial functionality to the composite. GO itself has antibacterial properties and also provides the advantage of combining both Ag and IO NPs in a single composite. The GO-IO-Ag nanocomposite could be easily separated and recycled by magnetic separation, ideally for its further use in an economic and eco-friendly manner. With these benefits, the GO-IO-Ag nanocomposite produced in our study can be applied as a multifunctional antibacterial agent in various areas from healthcare to environmental remediation.

The novelty of the work is the green synthesis of the Ag NPs using cinnamon extract, which is a powerful antimicrobial agent as well. Multifunctional nanocomposite with antibacterial and magnetic properties is another feature of this work. We have compared the antibacterial properties of different samples

synthesized using Gram-negative bacteria *Escherichia coli* (*E. coli*) and Gram-positive bacteria *Staphylococcus aureus* (*S. aureus*) as model microorganisms.

2. Experimental

2.1. Reagents and materials

Iron(III) chloride hexahydrate ($FeCl_3.6H_2O$), iron(II) chloride tetrahydrate ($FeCl_2.4H_2O$), silver nitrate ($AgNO_3$) were purchased from purchased from Sigma Aldrich (Singapore). Water-soluble quaternized chitosan (CS) was purchased from G.T.C. Bio Corporation (China). Few-layered graphene oxide (GO) was purchased from Cheap Tubes Inc (USA). All other reagents used in this work were of analytical grade and purchased from Sigma Aldrich (Singapore) and directly used. Cinnamon powder was purchased from a local market (Singapore).

2.2. Green synthesis of Ag NPs, [GO + Ag], [GO + Ag@CS] nanocomposites

The Ag NPs were synthesized using cinnamon extract as the green reducing agent as shown in Scheme 1(a). For the preparation of the extract, 2 g of cinnamon powder was dispersed in 100 mL DI water in a conical flask and boiled for a few minutes and later cooled to room temperature. The dispersion was then filtered to obtain a clear solution of cinnamon extract, which was stored in refrigerator at 4 °C. The concentration of the cinnamon extract required for the reduction of $AgNO_3$ to Ag NPs and the time of synthesis were investigated and optimized. The clear filtered solution of cinnamon extract with different volume (50 µL to 2 mL) was added to $AgNO_3$ (5 mL, 1 mM) solutions in screw cap vials and stirred at room temperature for 24 h. The solution color changed from yellow to dark brown with an increase in cinnamon extract concentration (Scheme 1(a)) indicating the formation of NPs. The final product was centrifuged at 9,000 rpm for 20 min and washed twice with DI water.
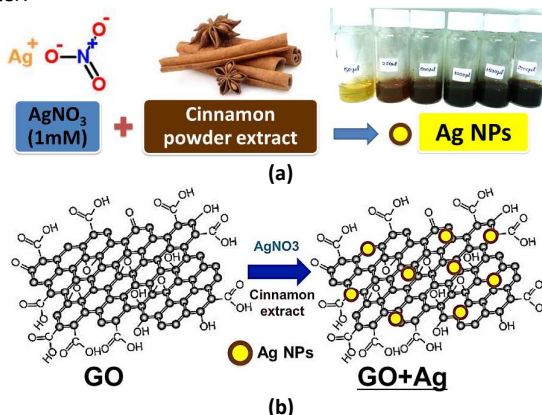
Scheme 1. Schematic showing the synthesis of Ag NPs (a) and [GO+Ag] nanocomposite (b).

For [GO+Ag] nanocomposite synthesis (Scheme 1(b)), GO was well dispersed in DI water (10 mg in 60 ml) by ultra-sonication, then 10 mg $AgNO_3$ was added to it, followed by the addition of cinnamon extract (18 ml) while stirring at high speed. The reaction mixture was kept stirring at room temperature for 24 h. The final product was filtered and washed several times with DI water. Later, the nanocomposite synthesized was freeze-dried.

The chitosan coated Ag NPs (Ag@CS) were also prepared by adding 1.5 mL of cinnamon extract and quaternized chitosan (6.92 mg, 10 mL) to $AgNO_3$ (5 mL, 1 mM) solution in DI water. This mixture was allowed to stir continuously at room temperature for 3 h to obtain a homogeneous solution and later incubated at 95 ^{o}C for 12 h. The solution colour changed from yellow to yellowish brown that confirmed the coating of chitosan (CS) to the Ag NPs. For synthesis of [GO + Ag@CS] nanocomposites, 5 mg of GO was dispersed in 5 mL of DI water by ultra-sonication, to which a 10 ml of the Ag@CS solution prepared above was added. The mixture was kept for overnight stirring, and then washed and freeze-dried.

2.3. Synthesis of IO NPs and [GO+IO] nanocomposite

The IO NPs were synthesized according to the co-precipitation method. $FeCl_3.6H_2O$ (5 mg) and $FeCl_2.4H_2O$ (2.5 mg) were added to 2.5 ml of DI water and kept under mechanical agitation in N_2 atmosphere (90° C, 20 min). Then, NH_3 (1 mL) was added drop wise and stirred for 4 h at 90° C. The resulting black precipitate was washed several times with DI water and kept for freeze-drying. For the synthesis of [GO+IO] nanocomposite, 2.5 mg GO was dispersed in 2.5 ml of DI water by ultra-sonication first. Then the salts, $FeCl_3$ (5 mg) and $FeCl_2.4H_2O$ (2.5 mg), were added to the GO dispersion in DI water (1 mg/ml), following the similar method described above for IO NPs (Scheme 2). The final product was filtered, washed at least 3 times by DI water and the precipitate was freeze-dried, and used for further characterizations.

2.4. Synthesis of [GO+IO+Ag] nanocomposite

In this case, the [GO+IO] nanocomposite prepared in section 2.3 was used as the starting base and Ag NPs were synthesized *in-situ* as shown in Scheme 2. For the *in-situ* synthesis of Ag NPs, 1 mg of [GO+IO] was homogeneously dispersed in 13 ml of DI water first and then 3 mg of $AgNO_3$ was added. Next, 5 ml of cinnamon extract was added and the reaction mixture was left for stirring overnight. The resulting mixture was washed and freeze-dried.
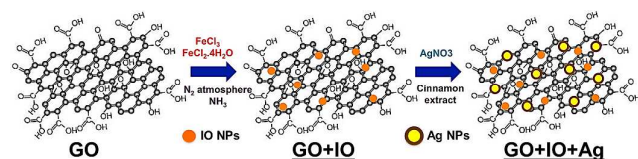
Scheme 2 Schematic showing the synthesis of [GO+IO] and [GO+IO+Ag] nanocomposites.

2.5. Characterization

The UV-vis absorbance of the samples was measured using UV-VIS-NIR Spectrophotometer UV-3600 (Shimadzu) to confirm the formation of Ag NPs. TEM and EDX analysis was carried out using a 200 kV JEOL (Tokyo, Japan) transmission electron microscope. Crystallinity, structure, and crystallite size of NPs were determined by the X-ray diffraction (XRD) using a Rigaku (Tokyo, Japan) Miniflex X-ray diffractometer with Cu-Kα radiations (λ = 0.15406 nm) in the 2θ range from 20° to 90°. Fourier transform infrared (FTIR) spectra of the samples were obtained using a PerkinElmer (Waltham, MA) FTIR spectrophotometer in the KBr matrix. A 40 ± 5% kHz Panasonic-mini ultrasonic water bath and also a tip sonication (QSONICA sonicators) were used for dispersion of the NPs when necessary.

2.6. Antibacterial testing protocols

Preparation of working cultures: *E. coli* ATCC 25922 and *S. aureus* ATCC 29213 were maintained on LB agar. Before the experiment, overnight cultures of bacteria were prepared by inoculating 2-3 bacteria colonies into 5 ml of Tryptic soy broth and incubated overnight at 37 °C for about 16 h in a shaker. A volume of 500 µl of overnight culture was then used to inoculate 50 ml of fresh tryptic soy broth and incubated at 37 °C for about 3 h under shaking conditions to obtain a mid-log phase. The mid-log phase culture was further diluted with fresh Mueller Hinton (MH) broth to an optical density (Lambda = 600 nm) of 0.25 ± 0.01 for *E. coli* and to 0.40 ± 0.01 for *S. aureus*. These optical densities corresponded to the bacteria count of approximately 1-2 x 10^8 CFU/ml. The cultures of bacteria were further diluted by 1:100 with MH broth to obtain the working culture with a bacterial count of 1-2 X 10^6 CFU/ml.

Preparation of serial dilution of test samples and minimum inhibitory concentration (MIC) assay: Antibacterial activities against Gram positive (*S. aureus*) and Gram negative (*E. coli*) bacteria were tested using the protocol adapted from Wiegand *et al.*[48] We prepared aqueous dispersion of the NPs and nanocomposites at a concentration of 0.2 mg/ml. All samples were homogenized via a vortex mixer prior to dilution. A serial dilution was performed on each sample for 4 times. At each successive dilution, an aliquot of 1.5 ml of test sample was added into the next tube containing 1.5 ml of sterile MH broth and mixed thoroughly. Therefore, each successive dilution halved the concentration of the sample. Addition of working culture into each tube (1:1) diluted the sample further, generating an effective range of concentration. The effective bacteria count in each tube was estimated to be 10^5 CFU/ml. After the addition of working culture, the tubes were left for incubation at 37 °C overnight for at least 16 h. Then, those tubes were observed visually for turbidity, and the lowest concentration which showed no turbidity, indicating no bacteria growth, was taken as the minimum inhibitory concentration (MIC).

3. Results and discussion

3.1. Absorption characteristics

The formation of Ag and Ag@CS NPs was visually characterized by the colour of the solution transforming from yellow to dark brown. Scheme 1a shows the change in colour of the $AgNO_3$ solution with an increase in cinnamon extract concentration indicating the formation of Ag NPs. The formation of Ag NPs was further confirmed by the UV-vis spectra as shown in Fig. 1. UV-vis absorption spectra of Ag NPs and nanocomposites containing Ag presented a distinct surface plasmon resonance (SPR) absorption at around 430 nm. It should be noted that the absorbance is directly proportional to the concentration of Ag NPs. The increase in the absorbance values with increasing cinnamon extract dosage demonstrates the greater production of Ag NPs, which is because of the increased availability of the reducing biomolecules involved in the reduction of silver ions at higher dose of the extract. It can be concluded from Fig. 1a that the optimum amount of cinnamon extract is 1.5 mL for 5 ml of 1 mM of $AgNO_3$ solution and the time of reduction is 24 h.

The main phytochemicals in cinnamon is cinnamaldehyde.[38] In addition, cinnamon also contains tannins, flavonoids, glycosides, terpenoids and some proteins. It has been reported that the proteins can bind to the nanoparticles either through their free

amine groups or cysteine residues.[39,40] Terpenoids in plant extracts have shown to be vital in the synthesis of Ag NP via the reduction of Ag ions.[39] In another study, polyols such as terpenoids, flavones and polysaccharides in the cinnamomum camphora leaves have been reported to be key factors in the bioreduction of silver and chloroaurate ions.[41] For the hydrolysable tannins, it is possible that there is the formation of intermediate complexes with OH groups of the phenolic compounds, which undergo oxidation to quinine forms leading to the reduction of Ag^+ to Ag NPs.[42,43] Based on these reports, we suggest that the water-soluble fractions consisting of complex polyols in the cinnamon extract contribute to the reduction of Ag ions to Ag NPs. They also play a role in binding to the surface of the NPs and stabilizing them.

The Ag NPs produced from cinnnamon extract were observed to be very stable in the solution, even 1 month after their synthesis as indicated by the UV-vis spectra of the Ag NPs stored at room temperature (covered with a foil). The simplicity of the method, non-toxic cinnamon, neutral pH and room temperature conditions make this synthesis method suitable for biological studies and biomedical applications.

In addition to cinnamon, we have also used water-soluble quaternized chitosan (CS) to coat the Ag NPs. Importantly, chitosan possesses excellent biocompatibility, biodegradability, antibacterial property and metal binding ability.[44] The absorption peak at around 430 nm in the UV-vis spectrum (Fig. 1b) of the nanocomposite of [GO+Ag@CS] confirms the presence of Ag NPs.
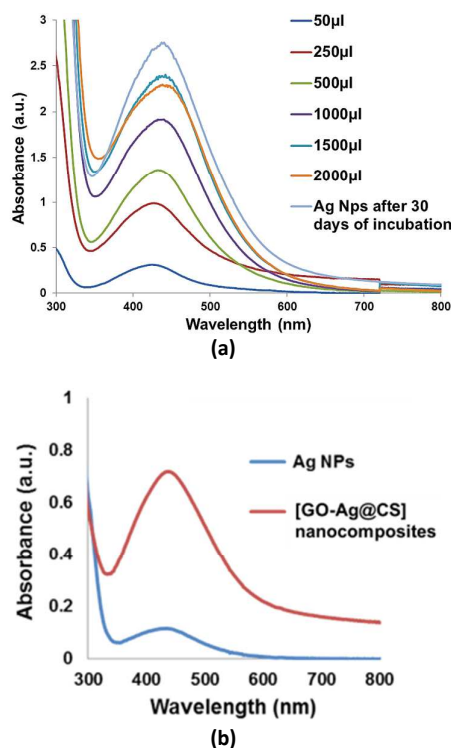

(a)

(b)

Fig. 1 UV-vis absorption spectra of (a) fresh Ag NPs with different volume of cinnamon extract (50 µL to 2 mL) and after 30 days of ageing, and (b) [GO-Ag@CS] nanocomposites.

3.2. TEM

The TEM images of the Ag NPs and the nanocomposites are shown in Fig. 2. It is revealed from the images that the average diameter of

Ag NPs is around 20-30 nm and they are uniform and evenly distributed on the GO sheet in the [GO-Ag@CS] nanocomposite. On the other hand, IO NPs are smaller than Ag NPs and the average size is around 5 nm. They are well dispersed along the GO sheet. From Fig. 3 the presence of IO and Ag NPs on the GO sheet can be clearly seen and is also confirmed by the energy-dispersive X-ray spectroscopy (EDX) analysis, showing peaks from Fe, O and Ag. The peak for C comes from GO as we use mesh type copper grid to avoid C and Cu peaks from the background grid. EDX spectroscopy results confirm the significant presence of pure 100% Fe, O and Ag with no other contaminants. The size and the contrast of the IO and Ag NPs are different with Ag NPs being bigger and darker compared to IO NPs. However, both these NPs are uniformly spread on the GO sheet in the composite.
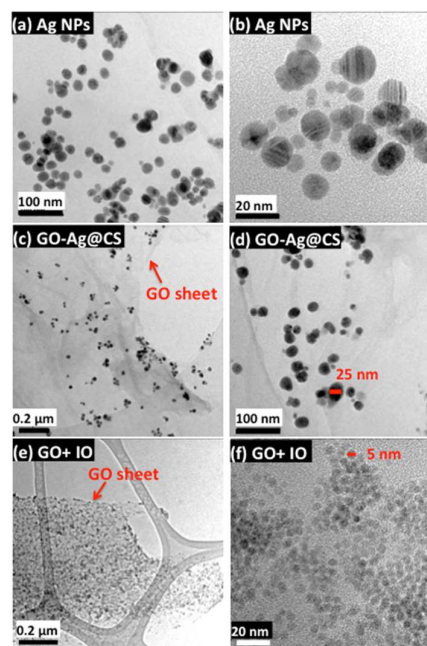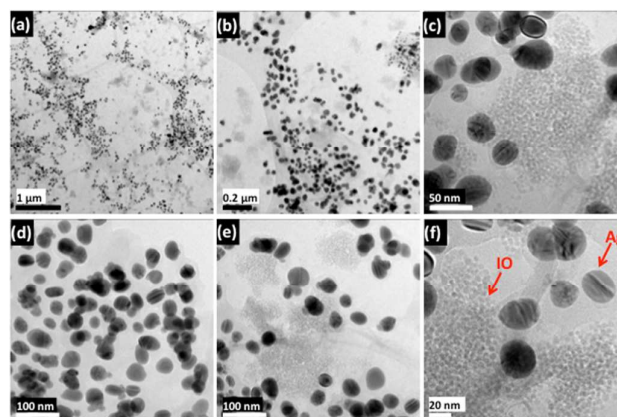

Fig. 2 TEM images of (a, b) Ag NPs synthesized using cinnamon, and nanocomposites of (c, d) [GO+Ag@CS] and (e, f) [GO+IO].
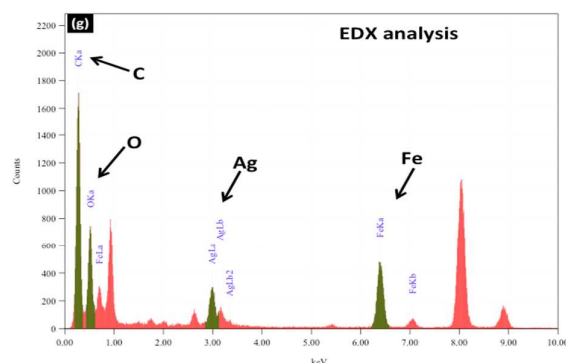
Fig. 3 **(a-f)** TEM images and **(g)** the energy-dispersive X-ray spectroscopy (EDX) analysis of the nanocomposite of GO, IO and Ag NPs [GO+IO+Ag] indicating the presence of both Ag and IO NPs on the GO sheet.

3.3. XRD

The XRD profiles of GO sheets, IO NPs, Ag NPs and [GO+IO+Ag] nanocomposite are shown in Fig. 4. The XRD patterns of IO NPs and nanocomposite present the diffraction angles at 35.8°, 43.5°, 54°, 57.5° and 63° which implies the diffraction surfaces of the cubic unit cell of magnetite (Fe_3O_4) nanocrystal. This data is in good agreement with the standard data of Fe_3O_4 NPs from the American Society for Testing and Materials (ASTM) and International Centre for Diffraction Data (ICDD: 750449).[31] Ag NPs have shown clear peaks of cubic phases (JCPDS No. 03-0921) at 2θ of 38°, 44°, 64.4° and 77.6°. However, some minor peaks representing the hexagonal phases (JCPD No. 41-1402) at 45.9°, 57.9° and 76.0° were also noticed. It implies that the synthesized Ag NPs are biphasic in nature. The distinctive feature of the nanocrystallites is the presence of strain in the crystal structure, which was indicated by the slight shift in the peak positions.[45] The XRD pattern of the nanocomposite shows clearly the presence of metallic Ag. It also confirms the presence of Fe_3O_4 NPs. It is inferred from XRD patterns that as-synthesized composite materials exhibit good crystallinity and high purity. It is noticed that, except for the peaks assigned to Fe_3O_4 and Ag NPs, no obvious diffraction peak has resulted from GO, which indicates that the stacking of GO sheets in the composite is disordered.[46]
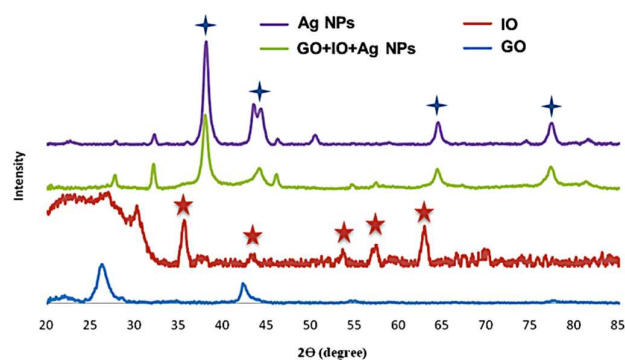

Fig. 4 XRD patterns of GO sheets, IO NPs, Ag NPs and nanocomposite [GO+IO+Ag].

3.4. FTIR

Fig. 5 shows the FTIR spectra of GO sheets, Ag NPs, IO NPs, and [GO+Ag+IO] nanocomposites. The presence of different types of oxygen functionalities in GO is evident from peaks corresponding to oxygen stretching vibration (2900–3600 cm^{-1}, O–H stretching vibration) and C=O stretching vibration (1650 cm^{-1}).[47] The FTIR spectrum of IO NPs exhibited vibrations in the region 400–700 cm^{-1}, which can be assigned to the vibrations of Fe–O.[48]

As seen from Fig. 5, the cinnamon extract has peaks at 1763 and 1658 cm^{-1}, which correspond to stretching vibrations of cinnamaldehyde, a major component of the cinnamon extract. The peaks at 1567 and 1475 cm^{-1} correspond to an aromatic ring and C–OH bending, respectively[49] and those from 3600–3200 cm^{-1} can be assigned to the O–H stretch for alcohols and phenols present in cinnamon.[50] The FTIR spectra for the Ag NPs indicated the presence of peaks very similar to the ones present in the FTIR spectra of cinnamon extract. This observation indicates that the cinnamon extract acts not only as a reducing agent but also as a capping agent. This capping of Ag NPs with cinnamon is responsible for the stability of Ag NPs as indicated by the UV-vis spectra.
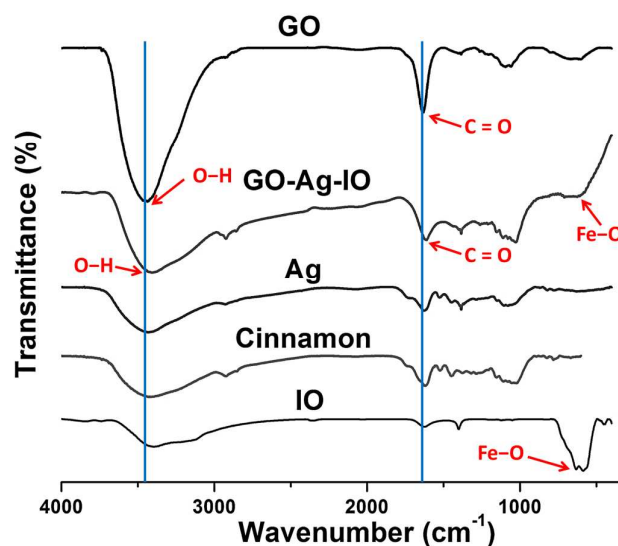

Fig. 5 FTIR spectra of GO sheets, nanocomposite [GO+IO+Ag], Ag NPs synthesized using cinnamon extract, cinnamon and IO NPs**.**

Comparing the FTIR spectra of GO, IO and Ag NPs with the [GO+IO+Ag] nanocomposite, the presence of IO is clearly indicated by presence of peaks in the 400–700 cm^{-1} region. The peaks corresponding to O–H and C=O stretching vibration are also present in the [GO+IO+Ag] nanocomposite indicating the presence of GO and Ag NPs. It should be noted that there is a shift of C=O stretching vibration band to a lower wavenumber (1638 cm^{-1}) in the case of the nanocomposite, which indicates strong interaction (H-bonding) between the capping agent (cinnamon extract) and the GO sheets. This interaction is also validated by the shift in the O–H stretching peak to a lower wavenumber as seen from Fig. 5.

3.5. Antibacterial properties

The antibacterial properties are evaluated by comparing the MIC values for different samples against Gram-negative *E. coli* and Gram-positive *S. aureus* (Table 1 and Fig. 6). Figs 6a and 6b show

Please do not adjust margins

RSC Advances

the MIC assays for different nanoparticles and nanocomposites against *E. coli* and *S. aureus*, respectively. The positive control (MH liquid media without any active substance) shows the turbidity, indicating the proliferation of bacteria. On the other hand, the sterility control without any active substance is clear, demonstrating no bacterial growth. Among all different nanoparticles (IO, Ag), GO sheets and nanocomposites ([GO+IO], [GO+Ag], [GO+Ag@CS], [GO+IO+Ag NPs]) tested, the Ag NPs and [GO+Ag@CS], [GO+IO+Ag NPs] nanocomposites exhibit a lower MIC of 0.025 against *E. coli*. On the contrary, these nanocomposites exhibit a higher MIC of 0.05 against *S. aureus* (Table 1). Whilst, GO (commercial), IO NPs and [GO+IO] nanocomposites exhibit a higher MIC of > 0.1 against both bacterial strains.

The above differences in the antimicrobial activity of the samples observed could be related to the difference in structure of the cell walls of the two types of bacteria.[51] The cell wall of *E. coli* bacteria is made up of a thin peptidoglycan layer and a lipopolysaccharide layer.[52] The lipopolysaccharides consist of covalently linked lipids and polysaccharides exhibiting a negative charge, which serves as a weak permeability barrier to the Ag NPs and the nanocomposites having a positive charge. On the other hand, the cell wall of *S. aureus* bacteria is made up of a thick peptidoglycan layer comprising of linear polysaccharide chains cross-linked by short peptides to form a three dimensional rigid structure.[52] This rigid layer in turn restricts the attachment or penetration of the Ag NPs and the nanocomposites to the cell wall.

Our MIC assays clearly validate the above discussion. It is also clear from Fig. 6 that the bacterial cell killing efficiency gradually increases and hence, the culture media becomes clearer with the increasing concentration of the samples containing Ag. Our MIC results for Ag NPs are found to better than the values reported in the literature review by Hajipour *et al.*[53] This is attributed to the presence of cinnamon extract which also has some antibacterial properties. This synergistic effect leads to an enhanced antibacterial activity of the Ag NPs prepared with cinnamon.

3.5.1. Mechanistic antimicrobial activity of Ag

Several mechanistic studies of the antibacterial effect of Ag on different bacterial strains have been illustrated in the literature. Feng *et al.* proposed a mechanistic study and correlated the antibacterial effect to the detachment of cytoplasm membrane from the cell wall.[54] They have also confirmed the loss of replication ability of DNA and the inactivation of protein. Shrivastava *et al.* proposed a mechanism whereby the interaction of bacterial cell wall with Ag NPs resulted in perforations that were responsible for the antibacterial effects of the nanoparticles.[51] They also suggested that the bacterial growth signalling pathway was impeded by Ag NPs through the modulating tyrosine phosphorylation of putative peptide substrates critical for cell viability and division. Another mechanism suggested that the association of silver with oxygen and its reaction with sulfhydryl (–S–H) groups on the cell wall formed R–S–S–R bonds that blocked the respiration and caused cell death.[55] Similar modes of action for Ag NPs and Ag ions have been reported by Cho *et al.*[56]

Table 1. Antibacterial activity of different samples against Gram negative bacteria (*E. coli*) and Gram positive bacteria (*S. aureus*) with minimum inhibitory concentration (MIC) values. Initial inoculum: 5 X 10^5 CFU/mL.

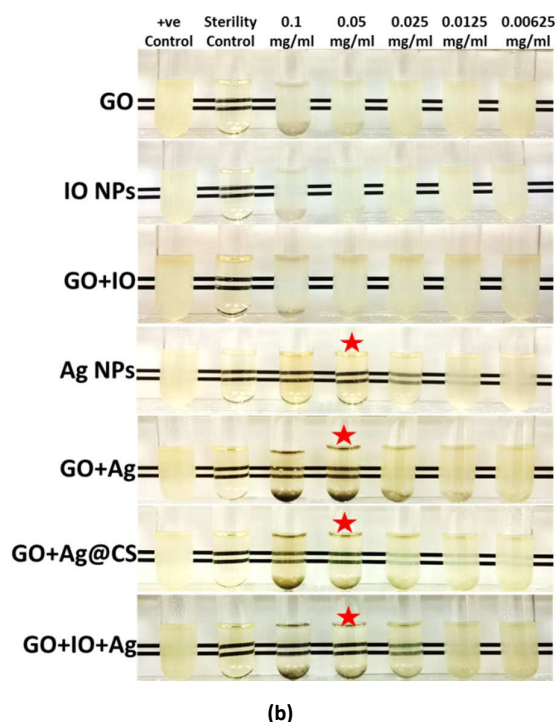|	MIC (mg/ml) against *E. coli*	MIC (mg/ml) against *S. aureus*
GO (Commercial)	> 0.1	> 0.1
IO NPs	> 0.1	> 0.1
GO + IO	> 0.1	> 0.1
Ag NPs	0.025	0.05
GO + Ag	0.05	0.05
GO + Ag@CS	0.025	0.05
GO + IO + Ag NPs	0.025	0.05

(a)

Please do not adjust margins

(b)
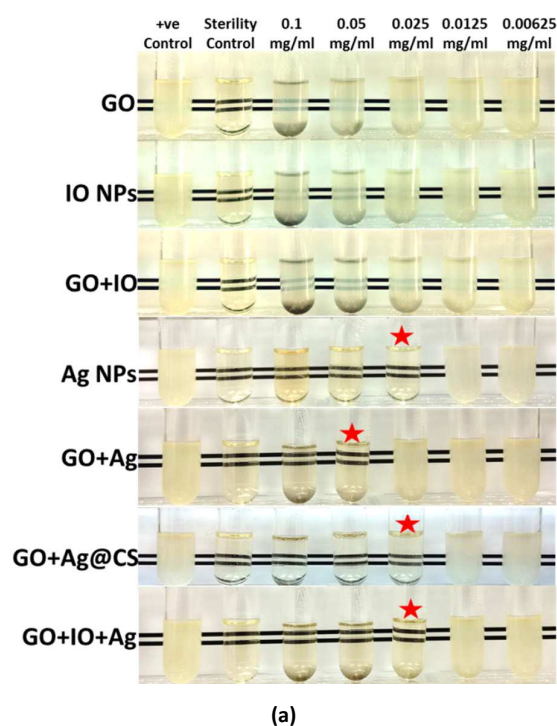
Fig. 6 Photographs showing the minimum inhibitory concentration (MIC) values of different samples (highlighted with star) against **(a)** Gram negative bacteria (*E. coli*) and **(b)** Gram positive bacteria (*S. aureus*).

3.5.2. Mechanistic antimicrobial activity of GO and IO

It is interesting to note that [GO+Ag@CS] and [GO+IO+Ag] nanocomposites exhibit the same antibacterial activities as Ag NPs. The relative percentage of Ag is low in these two nanocomposite compared to Ag NPs alone. GO and IO NPs also have antibacterial effect but not as good as Ag NPs. Our results suggest that the nanocomposites prepared are as effective as Ag NPs and the different components (GO, Ag, IO) work together in synergy to create the enhanced antibacterial effect.

The main mechanism for the antibacterial activity of GO is related to its physical and chemical properties and has been reported to be the synergistic effects of membrane disruption of the cell envelope and oxidative stress.[23] Chen *et al.* reported that the bacterial cells were intertwined with GO sheets and resulted in local perturbation of the cell membrane, which brought about the loss of the bacterial membrane potential and hence, leakage of electrolytes, and finally led to the lysis and death of pathogens.[57] The main mechanism by which the IO NPs show antibacterial activity might be via oxidative stress generated by reactive oxygen species (ROS).[26,27] ROS can cause damage to proteins and DNA in bacteria. It has also been reported that the smaller size of the NPs is responsible for the bactericidal effects. In one study, Lee *et al.* have shown that the penetration of the small iron NPs particles (sizes ranging from 10 - 80 nm) into the *E. coli* membranes led to the inactivation of the bacteria.[58] Later, the nano-scale iron could react with the intracellular oxygen and cause the oxidative stress and ultimately lead to the disruption of the cell membrane.

3.6. Antibacterial and magnetic nanocomposites

In addition to the antibacterial properties, the nanocomposite containing IO NPs can be utilized for magnetic based separation studies. Fig. 7 shows the digital photographs of [GO+IO+Ag] nanocomposites dispersed in water before and after magnetic separation. Upon magnetic separation, all particles are harvested, leaving behind a clear solution, confirming the fact that both magnetic and antibacterial properties are preserved in the nanocomposite. This opens up new avenues in theranostic applications.
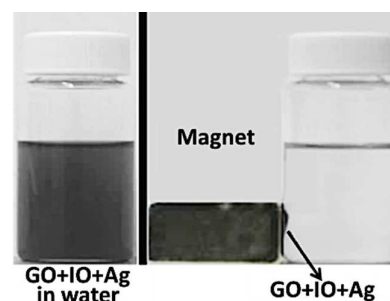

Fig. 7 Photograph showing the dispersion of [GO+IO+Ag] nanocomposites in water (left image) and the magnetic separation using an external magnet (right image).

It has become a major concern to eradicate antibiotic-resistant bacteria using multiple costly drugs that may have side effects. Consequently, treatments are expensive and time consuming. The nanocomposites developed in our study could offer a new strategy to tackle multidrug-resistant bacteria. The additional magnetic property will make their targeting and separation easier. Besides, they can also be applied in the field of water purification, food packaging and antimicrobial surfaces.

4. Conclusions

We have demonstrated a facile green synthesis of Ag NPs with excellent antibacterial properties by using cinnamon extract as a reducing agent. We believe that this method could reduce the usage of expensive Ag salts and NPs without compromising the antibacterial effect through the synergistic action of cinnamon and very low concentration of Ag salts used in our NPs synthesis. We have also developed green methods using cinnamon and chitosan for a variety of nanocomposites containing Ag, IO and GO. Of particular interest, [GO+IO+Ag] nanocomposites are bi-functional and exhibit both antibacterial and magnetic properties.

Acknowledgements

References

1   R. Dastjerdi and M. A. Montazer, *Colloids Surf. B*, 2010, **79**, 5–18.

RSC Advances Accepted Manuscript

2   T. Tian, X. Shi, L. Cheng, Y. Luo, Z. Dong, H. Gong, L. Xu, Z. Zhong, R. Peng and Z. Liu, *ACS Appl. Mater. Interfaces*, 2014, **6**, 8542–8548.

3   Y. Qiao, C. Yang, D.J. Coady, Z.Y. Ong, J.L. Hedrick, and Y.-Y. Yang, *Biomaterials*, 2012, **33**, 1146–1153.

4   H. H. Lara, E. N. Garza-Treviño, L. Ixtepan-Turrent and D. K. Singh, *J. Nanobiotechnol.*, 2011, **9**, 30.

5   M. Guzman, J. Dille and S. Godet, *Nanomed Nanotechnol*, 2012, **8**, 37–45.

6   C. P. Randall, L. B. Oyama, J. M. Bostock, I. Chopra and A. J. O ' Neill, *J. Antimicrob. Chemother.*, 2013, **68**, 131–138.

7   M. Saravanan, A. K. Vemu and S. K. Barik, *Colloids Surf., B*, 2011, **88**, 325–331.

8   A. Nanda and M. Saravanan, *Nanomedicine: Nanotechnology, Biology, and Medicine*, 2009, **5**, 452–456.

9   M. Saravanan and A. Nanda, *Colloids Surf. B*, 2010, **77**, 214–218.

10   A. J. Kora and J. Arunacahalam, *World J. Microbial. Biotechnol.*, 2011, **27**, 1209–1216.

11   N. M. Huang, H. N. Lim, S. Radiman, P. S. Khiew, W. S. Chiu, R. Hashim and C. H. Chia, *Colloids Surf., A*, 2010, **353**, 69–76.

12   A. Nabikhan, K. Kandasamy, A. Raj and N. M. Alikunhi, *Colloids Surf., B*, 2010, **79**, 488–493.

13   V. Alt, T. Bechert, P. Steinrucke, M. Wagener, P. Seidel, E. Dingeldein, E. Domann and R. Schnettler, *Biomaterials*, 2004, **25**, 4383–4391.

14   W. K. Jung, H. C. Koo, K. W. Kim, S. Shin, S. H. Kim and Y. H. Park, *Appl. Environ. Microbiol.*, 2008, **74**, 2171–2178.

15   A. B. Smetana, K. J. Klabunde, G. R. Marchin and C. M. Sorensen, *Langmuir*, 2008, **24**, 7457–7464.

16   A. Panacek, L. Kvitek, R. Prucek, M. Kolar, R. Vecerova, N. Pizurova, V. K. Sharma, T. Nevecna and R. Zboril, *J. Phys. Chem. B*, 2006, **110**, 16248–16253.

17   N. Gao, Y. Chen and J. Jiang, *ACS Appl. Mater. Interfaces*, 2013, **5**, 11307–11314.

18   W. Hu, C. Peng, W. Luo, M. Lv, X. Li, D. Li, Q. Huang and C. Fan, *ACS Nano*, 2010, **4**, 4317–4323.

19   O. Akhavan and E. Ghaderi, *ACS Nano*, 2010, **4**, 5731–5736.

20   M. R. Das, R. K. Sarma, R. Saikia, V. S. Kale, M. V. Shelke and P. Sengupta, *Colloids Surf., B*, 2011, **83**, 16–22.

21   S. Park, N. Mohanty, J. W. Suk, A. Nagaraja, J. An, R. D. Piner, W. Cai, D. R. Dreyer, V. Berry and R. S. Ruoff, *Adv. Mater.*, 2010, **22**, 1736–1740.

22   O. Akhavan and E. Ghaderi, *J. Phys. Chem. C*, 2009, **113**, 20214–20220.

23   S. B. Liu, T. H. Zeng, M. Hofmann, E. Burcombe, J. Wei, R. R. Jiang, J. Kong and Y. Chen, *ACS Nano*, 2011, **5**, 6971–6980.

24   L. H. Reddy, J. L. Arias, J. Nicolas and P. Couvreur, *Chem. Rev.*, 2012, **112**, 5818–5878.

25   J. S. Beveridge, J. R. Stephens and M. E. Williams, *Annu. Rev. Anal. Chem.*, 2011, **4**, 251–273.

26   M. A. M. Gijs, F. Lacharme and U. Lehmann, *Chem. Rev.*, 2010, **110**, 1518–1563.

27   M.-C. Wu, A. R. Deokar, J.-H. Liao, P. Y. Shih and Y. C. Ling, *ACS Nano*, 2013, **7**, 1281–1290.

28   A. Dong, Y. Sun, S. Lan, Q. Wang, Q. Cai, X. Z. Qi, Y. L. Zhang, G. Gao, F. Q. Liu and C. Harnoode, *ACS Appl. Mater. Interfaces*, 2013, **5**, 8125–8133.

29   T. Mosaiab, C. J. Jeong, G. J. Shin, K. H. Choi, S. K. Lee, I. Lee, I. In and S. Y. Park, *Mater. Sci. Eng. C*, 2013, **33**, 3786–3794.

30   H. Dong, J. Huang, R. R. Koepsel, P. Ye, A. J. Russell and K. Matyjaszewski, *Biomacromolecules*, 2011, **12**, 1305–1311.

31   S. S. Behera, J. K. Patra, K. Pramanik, N. Panda and H. Thatoi, *World J. Nano Sci. Eng.*, 2012, **2**, 196–200.

32   E. N. Taylor and T. J. Webster, *Int. J. Nanomed.*, 2009, **4**, 145–152.

33   A. M. Prodan, S. L. Iconaru, C. M. Chifiriuc, C. Bleotu, C. S. Ciobanu, M. Motelica-Heino, S. Sizaret and D. Predoi, *J. Nanomater.*, 2013, Article ID 893970.

34   M. Mohapatra and S. Anand, *Int. J. Eng. Tech.*, 2010, **2**, 127–146.

35   S. A. Mahdy, Q. J. Raheed and P. T. Kalaichelvan, *Int. J. M. Eng. Res.*, 2012, **2**, 578–581.

36   N. Tran, A. Mir, D. Mallik, A. Sinha, S. Nayar and T. J. Webster, *Int. J. Nanomed.*, 2010, **5**, 277–283.

37   S. Prabuseenivasan, M. Jayakumar and S. Ignacimuthu, *BMC Complement Altern. Med.*, 2006, **6**, 39.

38   K. Jayaprakasha, L. J. Rao and K. K. Sakariah, *Z. Naturforsch. C*, 2002, **57**, 990–993.

39   S. S. Shankar, A. Ahmad and M. Sastry, *Biotechnol. Prog.*, 2003, **19**, 1627–1631.

40   A. Gole, C. V. Dash, V. Ramachandran, A. B. Mandale, S. R. Sainkar, M. Rao and M. Sastry, *Langmuir*, 2001, **17**, 1674–1679.

41   J. Huang, Q. Li, D. Sun, Y. Lu, Y. Su, X. Yang, H. Wang, Y. Wang, W. Shao, N. He, J. Hong and C. Chen, *Nanotechnology*, 2007, **18**, 105104–105115.

42   A. D. Dwivedi and K. Gopal, *Colloids Surf., A*, 2010, **369**, 27–33.

43   A. Kumar, Y. Chisti and U. Chand, *Biotechnol. Adv.*, 2013, **31**, 346–356.

44   M. Kong, X. G. Chen, K. Xing and H.J. Park, *Int. J. Food Microbiol.*, 2010, **144**, 51–63.

45   M. Sathishkumar, K. Sneha, S. W. Won, C.-W. Cho, S. Kim and Y.-S. Yun, *Colloid. Surf., B*, 2009, **73**, 332–338.

46   M. Z. Kassaee, E. Motamedi and M. Majdi, *Chem. Eng. J.*, 2011, **172**, 540–549.

47   T. N. Narayanan, B. K. Gupta, S. A. Vithayathil, R. R. Aburto, S. A. Mani, J. Taha-Tijerina, B. Xie, B. A. Kaipparettu, S. V. Torti and P. M. Ajayan, *Adv. Mater.*, 2012, **24**, 2992–2998.

48   A. Azam, A. S. Ahmed, M. Mohammad Oves, M. S. Khan, S. S. Habib and A. Memic, *Int. J. Nanomed.*, 2012, **7**, 6003–6009.

49   Y. Q. Li, D. X. Kon and H. Wu, *Ind. Crops and Prod.,* 2013, **41**, 269–278.

50   B. Adinew, *Int. J. Herb. Medicine*, 2014, **1**, 22–31.

51   S. Shrivastava, T. Bera, A. Roy, G. Singh, P. Ramachandrarao and D. Dash, *Nanotechnology*, 2007, **18**, 225103–225111.

52   D. P. Tamboli and D. S. Lee, *J. Hazard. Mater.*, 2013, **260**, 878–884.

53   M. J. Hajipour, K. M. Fromm, A. A. Ashkarran, D. Jimenez de Aberasturi, I. R. de Larramendi, T. Rojo, V. Serpooshan, W. J. Parak and M. Mahmoudi, *Trends Biotechnol.*, 2012, **30**, 499–511.

54   Q. L. Feng, J. Wu, G. Q. Chen, F. Z. Cui, T. N. Kim, J. O. Kim, J *Biomed Mater Res*, 2000, **52**, 662–668.

55   V. S. Kumar, B. M. Nagaraja, V. Shashikala, A. H. Padmasri, S. S. Madhavendra, B. D. Raju, *J. Mol. Catal. A*, 2004, **223**, 313–319.

56   K. Cho, J. Park, T. Osaka and S. Park, *Electrochim. Acta*, 2005, **51**, 956–960.

57   J. Chen, H. Peng, X. Wang, F. Shao, Z. Yuan and H. Han, *Nanoscale*, 2014, **6**, 1879–1889.

58   C. Lee, J. Y. Kim, W. I. Lee, K. L. Nelson, J. Yoon and D. L. Sedlak, *Environ. Sci. Technol.*, 2008, **42**, 4927–4933.

RSC Advances Accepted Manuscript